Flow-Induced Vibration, Bearman (ed.) © 1995 Balkema, Rotterdam. ISBN 90 5410 547 X

Three-dimensional simulations of an oscillating rectangular cylinder

Tetsuro Tamura, Yoshiaki Itoh & Akira Wada
Tokyo Institute of Technology, Midori-ku, Yokohama, Japan

ABSTRACT: In order to understand the physical mechanism about the aeroelastic instability of bluff cylinders, the two-dimensional simulations have been mainly used for computational approach because the flow structure around the oscillating cylinder is expected to become two-dimensionalized due to the effects of the body motions. However, through the comparison with the experimental data, there is a little quantitative difference in the predicted values. We investigate the necessity of the three-dimensional simulation for the unsteady problems on forced-oscillating rectangular cylinders in uniform flow.

1. INTRODUCTION

For the physical understanding of fundamental aspects about the aeroelastic instability of bluff cylinders, the computational approach, which has some advantage to examine the detail of flow structures, has been applied to the unstable oscillations of a rectangular cylinder due to the coupling of vortex resonance and self-excited forces in a uniform flow. Thus far we have computed the two-dimensional incompressible flows around an oscillating rectangular cylinder which is mounted by the spring and the dash pot, and the aeroelastic characteristics have been qualitatively investigated for a rectangular cylinder. The reason for using two-dimensional simulations is that the flow structure around the cylinder becomes two-dimensionalized due to the oscillation. Certainly the computational results show that the coupling phenomena of the vortex-induced and the self-excited oscillations can be simulated[1]. We can also show by computation the branch off for the phenomena of nonlinear oscillations due to the initial conditions and the existence of the unstable limit cycle(Fig. 1). However, through the detailed comparison with the previous experimental data, there is a little quantitative difference in the predicted values each other. According to the three-dimensional computational result for the flow around the cylinder at rest, the vortex structures are distorted in the leeward region on the side and gradually changed due to the spanwise length and discretizations(Fig. 2). It is confirmed that the shear layer instability finally generate the three-dimensional structures in the near wake.

The objective of the present study is to clarify the necessity of the three-dimensional simulation of the aeroelastic problem. Accordingly we apply the direct finite difference technique[2],[3] of the three-dimensional incompressible Navier-Stokes equations to the unsteady flow problems on oscillating rectangular cylinders. Investigations are presented of the pressure fluctuations on the surface of the rectangular cylinder with side ratio equal to 2.0, which is forced to oscillate transverse to the approaching flow in heaving mode. In addition we discuss the possibility of the computational method to simulate the unsteady aerodynamic forces, whose accuracy and errors can be checked by examining the predicted values and the mechanism on the basis of the behavior of the shear layers and the wake structures of the cylinder.

2. PROBLEM FORMULATION

The interaction between the unsteady fluid flow and the dynamic behavior of a body plays an important role in decision of aerodynamic forces. The governing equations of the three-dimensional incompressible flow are given by the continuity equation and the Navier-Stokes equations as follows:

$$\frac{\partial \mathbf{u}}{\partial t} + (\mathbf{u} \bullet \text{grad})\,\mathbf{u} = -\text{grad}\, p + \frac{1}{Re}\Delta \mathbf{u}\,, \qquad (1)$$

$$D = \text{div}\,\mathbf{u} = 0\,, \qquad (2)$$

where $\mathbf{u}$, p, t and Re denote the velocity vector, pressure, time and the Reynolds number respectively, non-dimensionalized by U_0 (reference velocity), B (reference length), ρ (density) and ν (kinematic viscosity).

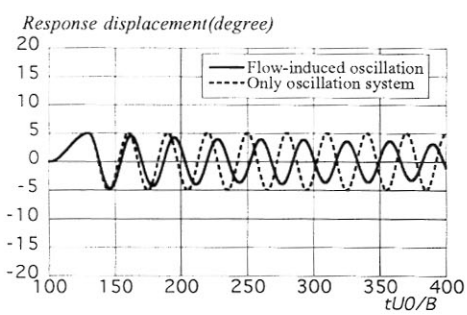

(a) initial displacement angle(5°)

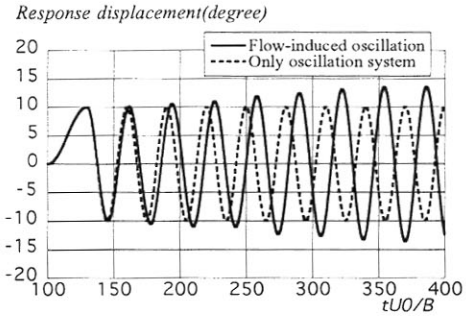

(b) initial displacement angle(10°)

Fig. 1 Branch off in 2-D simulation of freely- oscillating cylinder in uniform flow.

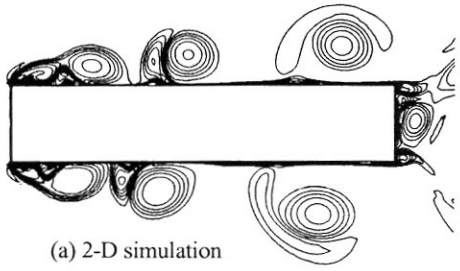

(a) 2-D simulation

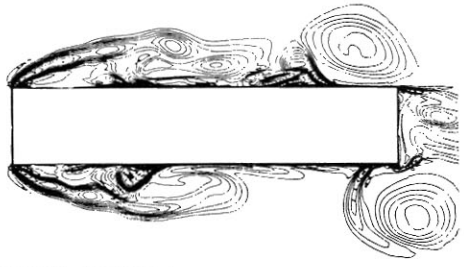

(b) 3-D simulation
(computational region: spanwise length=.25, increment=.05)

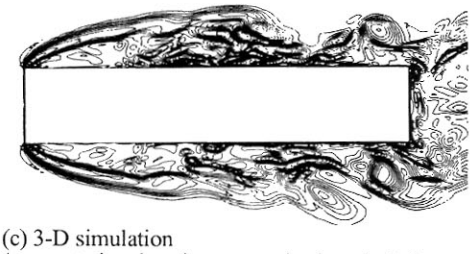

(c) 3-D simulation
(computational region: spanwise length=2.0, increment=.05)

Fig. 2 3-D simulation of the flow around a cylinder at rest.

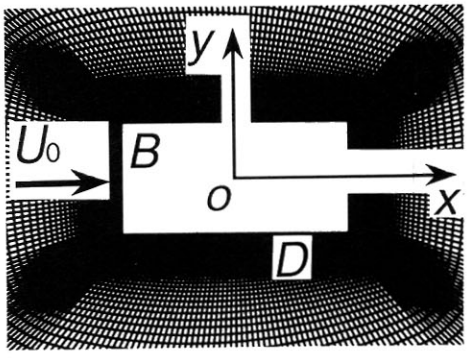

Fig. 3 Grid System for a rectangular cylinder

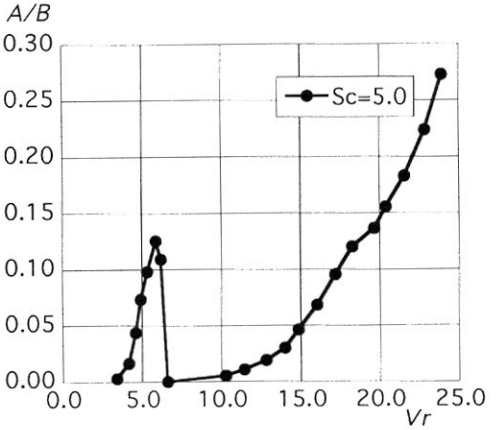

Fig. 4 Experimental response of the rectangular cylinder mounted elastically (D/B =2.0).

These equations are approximated by means of the finite difference method. In order to compute the unsteady flow around a moving body, the original governing equations are transformed by applying the generalized coordinate system including time[2]. The grid system of the physical domain moves with the motion of a body at each time step, although that of the computational domain is fixed. The computational domain is connected with the physical domain as:

$$\begin{aligned} \xi &= \xi(x,y,z,t)\,, \\ \eta &= \eta(x,y,z,t)\,, \\ \zeta &= \zeta(x,y,z,t)\,, \\ \tau &= t\,. \end{aligned} \tag{3}$$

The transformation of the coordinate derivatives is given based on (3) as follows:

$$\begin{aligned} f_\xi &= f_x x_\xi + f_y y_\xi + f_z z_\xi + f_t t_\xi\,, \\ f_\eta &= f_x x_\eta + f_y y_\eta + f_z z_\eta + f_t t_\eta\,, \\ f_\zeta &= f_x x_\zeta + f_y y_\zeta + f_z z_\zeta + f_t t_\zeta\,, \\ f_\tau &= f_x x_\tau + f_y y_\tau + f_z z_\tau + f_t t_\tau\,, \end{aligned} \tag{4}$$

where f_x stands for $\frac{\partial f}{\partial x}$ etc..
The time variable is treated as:

$$\tau = t\,, \tag{5}$$

accordingly

$$t_\tau = 1. \tag{6}$$

The time derivative is presented as:

$$f_\tau = f_x x_\tau + f_y y_\tau + f_z z_\tau + f_t\,. \tag{7}$$

The Navier-Stokes equations in the computational domain are rewrited as follows:

$$\frac{\partial \mathbf{u}}{\partial \tau} + \Big((\mathbf{u}-\mathbf{X}_\tau)\bullet \text{grad}\Big)\,\mathbf{u} = -\,\text{grad}\,p + \frac{1}{\text{Re}}\Delta\mathbf{u}\,, \tag{8}$$

where $\mathbf{X}_\tau$ stands for the velocity of the physical coordinate system (x_τ, y_τ, z_τ). This equation(8) means that the convection velocity in the computational domain is replaced by the relative velocity with respect to the moving coordinate system.

The time variable is specified to be constant for any space coordinates. Therefore the space derivatives of time should be equal to be zero in the computational domain as the following equation(9):

$$t_\xi = t_\eta = t_\zeta = 0 \tag{9}$$

Moreover as we only deal with the flow around the cylinder-type structure here, some geometric factors can be cancelled on the basis of the two-dimensional geometry. By the relation of equation(10), the conditions (11) can be obtained.

$$\zeta = \zeta(z) \tag{10}$$

$$z_\tau = z_\xi = z_\eta = x_\zeta = y_\zeta = 0 \tag{11}$$

As a result of applying the conditions (9) and (11), the first- and second-derivatives in space and the first-derivative in time are represented as the following equations (12),(13),(14),(15) and (16).

$$\begin{pmatrix} f_x \\ f_y \\ f_z \\ f_t \end{pmatrix} = \begin{pmatrix} y_\eta / J_* & -y_\xi / J_* & 0 & 0 \\ -x_\eta / J_* & x_\xi / J_* & 0 & 0 \\ 0 & 0 & 1/z_\zeta & 0 \\ \dfrac{\left(-y_\eta x_\tau + x_\eta y_\tau\right)}{J_*} & \dfrac{\left(y_\xi x_\tau - x_\xi y_\tau\right)}{J_*} & 0 & 1 \end{pmatrix} \begin{pmatrix} f_\xi \\ f_\eta \\ f_\zeta \\ f_\tau \end{pmatrix} \tag{12}$$

$$J_* = x_\xi y_\eta - y_\xi x_\eta \tag{13}$$

$$\begin{aligned} f_{xx} =& \frac{1}{J_*^2}\Big(y_\eta^2 f_{\xi\xi} - 2y_\xi y_\eta f_{\xi\eta} + y_\xi^2 f_{\eta\eta}\Big) \\ &+ \frac{1}{J_*^3}\Big(y_{\xi\xi} y_\eta^2 - 2y_\xi y_\eta y_{\xi\eta} + y_{\eta\eta} y_\xi^2\Big)\Big(f_\xi x_\eta - f_\eta x_\xi\Big) \\ &+ \frac{1}{J_*^3}\Big(x_{\xi\xi} y_\eta^2 - 2y_\xi y_\eta x_{\xi\eta} + x_{\eta\eta} y_\xi^2\Big)\Big(f_\eta y_\xi - f_\xi y_\eta\Big) \end{aligned} \tag{14}$$

$$\begin{aligned} f_{yy} =& \frac{1}{J_*^2}\Big(x_\eta^2 f_{\xi\xi} - 2x_\xi x_\eta f_{\xi\eta} + x_\xi^2 f_{\eta\eta}\Big) \\ &+ \frac{1}{J_*^3}\Big(y_{\xi\xi} x_\eta^2 - 2x_\xi x_\eta y_{\xi\eta} + y_{\eta\eta} x_\xi^2\Big)\Big(f_\xi x_\eta - f_\eta x_\xi\Big) \\ &+ \frac{1}{J_*^3}\Big(x_{\xi\xi} x_\eta^2 - 2x_\xi x_\eta x_{\xi\eta} + x_{\eta\eta} x_\xi^2\Big)\Big(f_\eta y_\xi - f_\xi y_\eta\Big) \end{aligned} \tag{15}$$

$$f_{zz} = \frac{1}{z_\zeta^2} f_{\zeta\zeta} - \frac{1}{z_\zeta^3} z_{\zeta\zeta} f_\zeta \tag{16}$$

The numerical procedures are based on the MAC method[4]. The regular mesh system is employed. All quantities are defined at the same location for a grid. The pressure field is determined by solving the Poisson equation as follows:

$$\Delta p = -\,\text{div}\Big(\Big((\mathbf{u}-\mathbf{X}_\tau)\bullet \text{grad}\Big)\,\mathbf{u}\Big) - \frac{\partial D}{\partial \tau} + \frac{1}{\text{Re}}\Delta D\,. \tag{17}$$

Providing that the effect of the viscous term is neglected at the high Reynolds number and the velocity vector of the next time step must satisfy the divergence-free condition, namely $D^{n+1} = 0$, the pressure equation is shown as follows:

$$\Delta p^{n+1} = -\,\mathrm{div}\,((\mathbf{u}^n - \mathbf{X}_\tau^{\,n})\bullet \mathrm{grad}\,)\mathbf{u}^n + \frac{D^n}{\delta\tau}, \quad (18)$$

where Δ, n and $\delta\tau$ are the Laplace operator, the time step and the non-dimensionalized time increment. The velocity field is computed by the semi-implicit temporal integration of the Navier-Stokes equations. The scheme is equivalent to the Euler backward scheme except the convection term.

$$\frac{\mathbf{u}^{n+1} - \mathbf{u}^n}{\delta\tau} + ((\mathbf{u}^n - \mathbf{X}_\tau^{\,n})\bullet \mathrm{grad}\,)\mathbf{u}^{n+1} = -\,\mathrm{grad}\,p^{n+1} + \frac{1}{\mathrm{Re}}\Delta\mathbf{u}^{n+1}, \quad (19)$$

where the convection term is linearized by use of the value at the previous time step for the convective velocity as follows:

$$(\mathbf{u} - \mathbf{X}_\tau)^{n+1}\cdot \mathrm{gradu}^{n+1} \doteqdot (\mathbf{u} - \mathbf{X}_\tau)^{n}\cdot \mathrm{gradu}^{n+1}. \quad (20)$$

Equations (18) and (19) are respectively solved at each time step by SOR method.

In order to overcome the numerical instability at high Reynolds numbers, the third-order upwind scheme is incorporated for the convection terms[5]. No turbulence model is adopted. For example,

$$\left(U\frac{\partial f}{\partial x}\right)_i = U_i\frac{-f_{i+2} + 8(f_{i+1} - f_{i-1}) + f_{i-2}}{12\delta x} + |U_i|\frac{f_{i+2} - 4f_{i+1} + 6f_i - 4f_{i-1} + f_{i-2}}{4\delta x} \quad (21)$$

3. COMPUTATIONAL MODEL

Fig. 3 displays a computational model. An rectangular cylinder has the depth-breadth ratio(D/B, D: the depth of a cylinder, B: the breadth) equal to 2.0. The cylinder is placed in the circular cylinder region(the diameter = $60B$, the height = B) for computation. The total number of the mesh points is 280x100x10 = 280000. The approaching flow is assumed to be uniform(U_0). The Reynolds number is equal to 10^4. For the boundary condition around the computational region, the Dirichlet condition is given for the velocity of in-flow and the Neumann condition is imposed for the velocity of out-flow and the pressure. On the surface of the cylinder, the velocity of the moving grid at boundary is given and the Neumann condition are employed for pressure. The the non-dimensionalized time increment is equal to 0.005.

4. FLOW PATTERNS AROUND AN OSCILLATING RECTANGULAR CYLINDER IN HEAVING MODE

Several types of the flow-induced instabilities are recognized for a rectangular cylinder as a function of the reduced velocity, $Vr = U0/Bfm$, where fm is cylinder oscillation frequency. According to the previous experimental data[6] in Fig. 4, under the conditions of D/B = 2.0 and the mass damping ratio of 5.0, the vortex-induced heaving oscillation and the galloping are observed at Vr = 3.5~6.5 and above Vr = 20.0 respectively. In order to examine the detailed flow pattern in aerodynamically unstable oscillations, three-dimensional simulations are carried out for a forced-oscillation of a rectangular cylinder in heaving mode($y0 = 0.1B$, $y0$: the amplitude of heaving oscillation). Oscillation displacement is shown as follows:

$$y(t) = y0*\sin(2\pi f_m t). \quad (22)$$

With regard to the reduced velocity, Vr = 5.5, 13.5 and 24.0 are selected for computation on the basis of the above experimental data.

The vorticity contours of horizontal section, the pressure contours of the side surface of the cylinder and the velocity vector fields of yz- section are illustrated in Figs. 5, 6 and 7 respectively. Instantaneous flow patterns of each reduced velocity are shown for three displacement phases of oscillation , namely $2\pi fmt$ = 0°, 90°, 180°. All flow patterns of three reduced velocities in Fig. 5 indicate that the vortex structures of $2\pi f_m t$ =0° are symmetrically same as that of $2\pi f_m t$ =180°. It can be realized that the cylinder oscillations almost control the separated flow from the leading edge and the wake.

Here the details of the flow patterns are examined for the respective reduced velocities as follows. In the case at Vr =5.5, it can be seen that the separated flow reattaches to the afterbody on the lower side surface of the cylinder at $2\pi f_m t$ = 0° and the separation bubble is generated. The formation of vortices, which stem from the motion of the cylinder, are recognized on the lower side at $2\pi f_m t$ = 90°.

According to the pressure contours of the side surface at Vr =5.5 in Fig. 6 it is found that the spanwize structures of pressure are two-dimensionalized. Especially the reattaching flow, which can be observed on the lower side at $2\pi fmt$ = 0°, make two-dimensional pressure structures on the side surface. On the other hand in case of more elongated rectangular cylinder(D/B=5.0) it was pointed out that the two-dimensional structures of the separated shear layer change into three-dimensional structures by the vortex instability[7]. They are quite different from each other on the reattached zone.

The three-dimensional structures of flow around the oscillating cylinder at Vr =5.5 are shown in Fig. 7. Inside the separation bubble, which can be observed

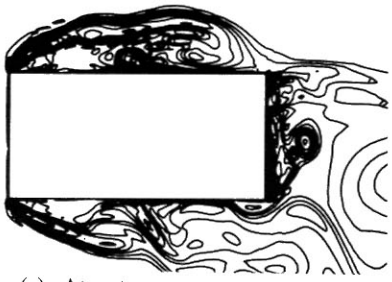

(a) At rest

(b) Vr = 5.5, $2\pi fmt$ =0°)

(c) Vr = 5.5, $2\pi fmt$ =90°)

(d) Vr = 5.5, $2\pi fmt$ =180°)

Fig. 5 Instantaneous vorticity contours in horizontal section

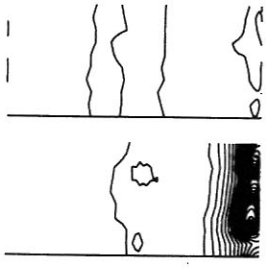

(a) At rest

(b) Vr = 5.5, $2\pi fmt$=0°)

(c) Vr = 5.5, $2\pi fmt$ =90°)

(d) Vr = 5.5, $2\pi fmt$ =180°)

Fig. 6 Instantaneous pressure contours on the side surface of a rectangular cylinder

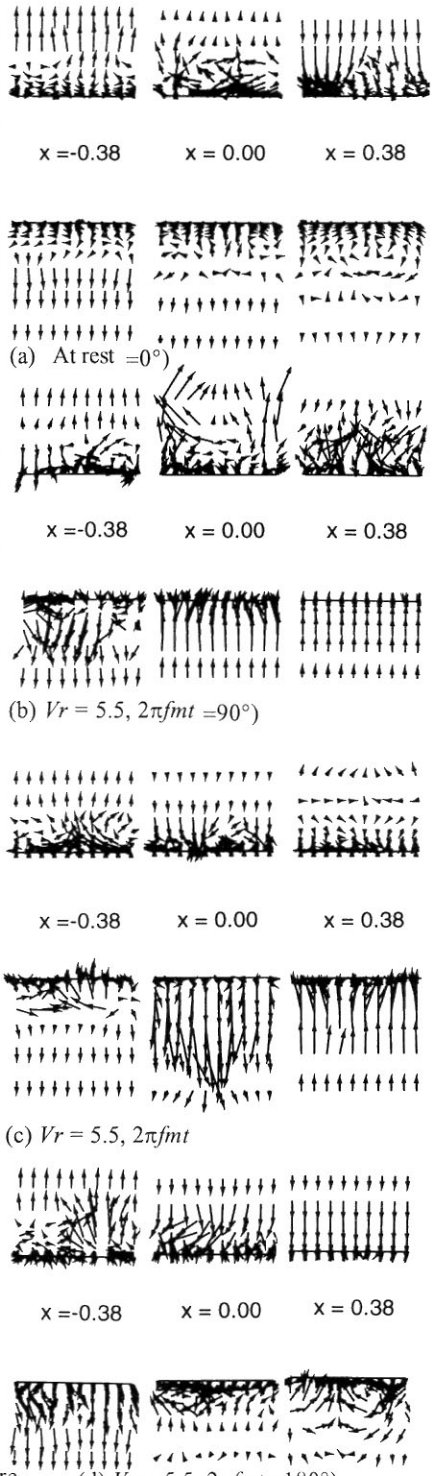

(a) At rest =0°)

(b) Vr = 5.5, $2\pi fmt$ =90°)

(c) Vr = 5.5, $2\pi fmt$

(d) Vr = 5.5, $2\pi fmt$ =180°)

Fig. 7 Instantaneous velocity vectors in yz-section

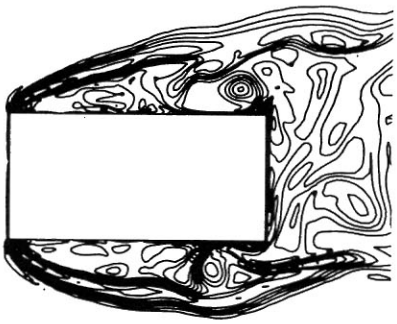

(e) Vr = 13.5, $2\pi fmt$ =0°)

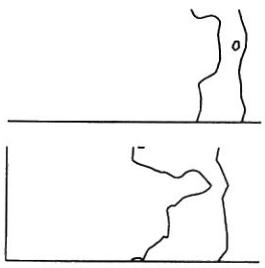

(e) Vr = 13.5, $2\pi fmt$ =0°)

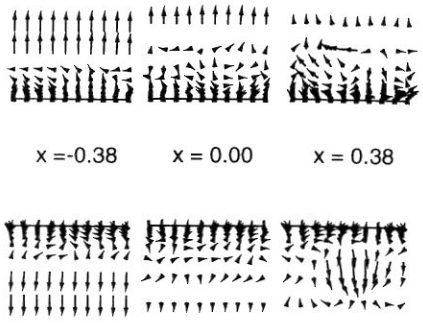

(e) Vr = 13.5, $2\pi fmt$ =0°)

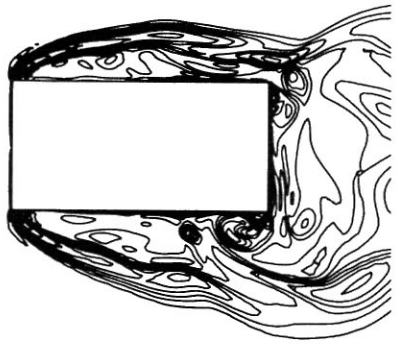

(f) Vr = 13.5, $2\pi fmt$ =90°)

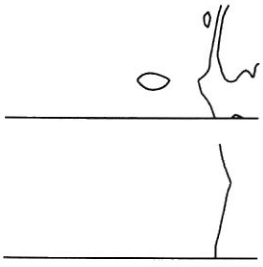

(f) Vr = 13.5, $2\pi fmt$ =90°)

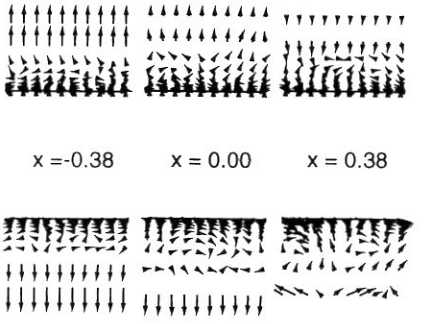

(f) Vr = 13.5, $2\pi fmt$ =90°)

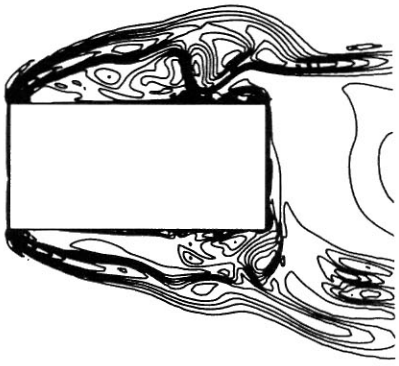

(g) Vr = 13.5, $2\pi fmt$ =180°)

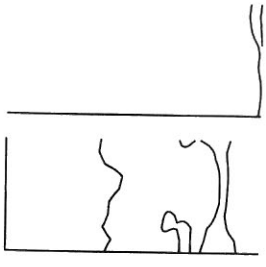

(g) Vr = 13.5, $2\pi fmt$ =180°)

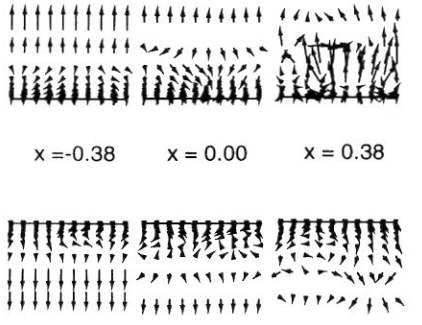

(g) Vr = 13.5, $2\pi fmt$ =180°)

Fig. 5 Instantaneous vorticity contours in horizontal section, continued

Fig. 6 Instantaneous pressure contours on the side surface of a rectangular cylinder , continued

Fig. 7 Instantaneous velocity vectors in yz-section , continued

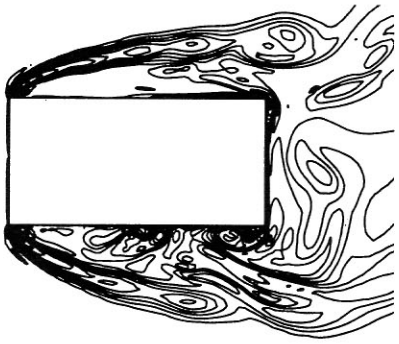

(h) Vr = 24.0, $2\pi fmt$ =0°)

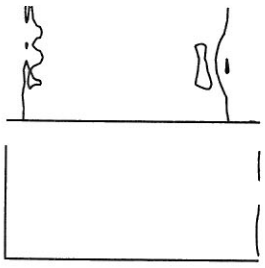

(h) Vr = 24.0, $2\pi fmt$ =0°)

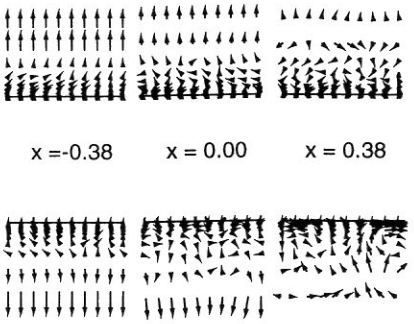

(h) Vr = 24.0, $2\pi fmt$ =0°)

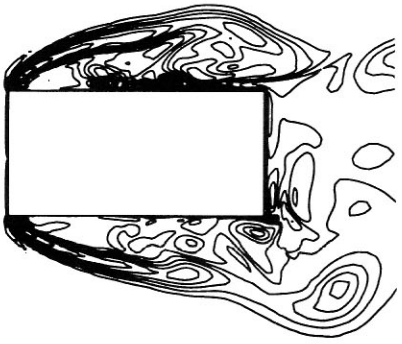

(i) Vr = 24.0, $2\pi fmt$ =90°)

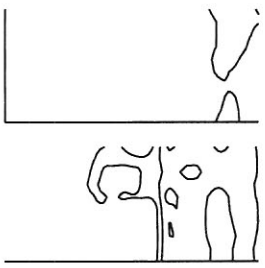

(i) Vr = 24.0, $2\pi fmt$ =90°)

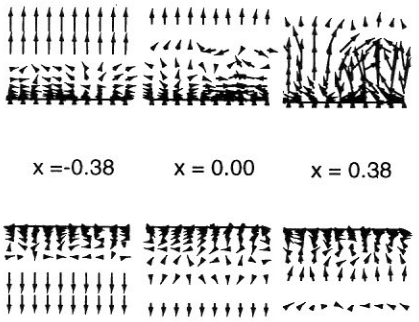

(i) Vr = 24.0, $2\pi fmt$ =90°)

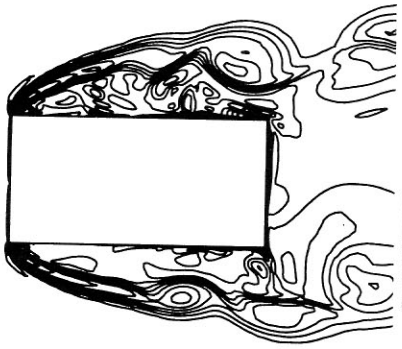

(j) Vr = 24.0, $2\pi fmt$ =180°)

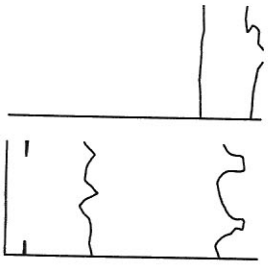

(j) Vr = 24.0, $2\pi fmt$ =180°)

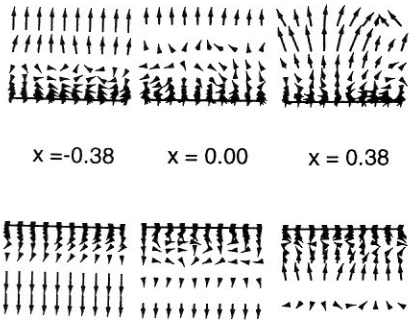

(j) Vr = 24.0, $2\pi fmt$ =180°)

Fig. 5 Instantaneous vorticity contours in horizontal section, continued

Fig. 6 Instantaneous pressure contours on the side surface of a rectangular cylinder , continued

Fig. 7 Instantaneous velocity vectors in yz-section , continued

on the lower side at $2\pi f_m t = 0°$, the velocity of z-direction, namely w is much larger than that of the other directions, nevertheless surface pressure is two-dimensional. On the other hand this remarkable three-dimensional structures of the separation bubble can not be observed at rest and the other reduced velocities. In these cases the velocities are lower inside the separated shear flow and the three-dimensional structures become to appear toward the leeward.

In the cases of Vr =13.5 and 24.0 of Fig. 5 the shear layers separated from the leading edge do not reattach to the afterbody and form the wide wake. Therefore the pressure distributions on the side surface in Fig. 6 are almost constant. The three-dimensionality of flow structures inside the separated flow gradually increases toward the leeward of the cylinder. The longitudinal vortices can be observed near the trailing edge of the cylinder. These are likely to the flow around a stationary cylinder.

The wake of the oscillating cylinder at Vr =13.5 is compared with that of Vr = 24.0 at $2\pi f_m t = 0°$. At Vr =13.5 the separated shear flow of the lower side is located closer to the side surface of the cylinder than that of the upper side. The wake of Vr =13.5 extends to the right upper side. On the other hand at Vr = 24.0 that of the upper side is closer than that of the lower side. The wake extends to right lower side.

As taking it into account that the cylinder is moving toward the upper side at $2\pi f_m t = 0°$, it is recognized that the behavior of the separated shear flow at Vr = 24.0 is consistent with the behavior obtained by the quasi-steady theory.

5. COMPARISON WITH EXPERIMENTAL DATA CONCERNING PRESSURE DISTRIBUTIONS

In this section, the distributions of the pressure on the side surface of a cylinder are compared with the previous experimental data[6]. Here the pressure coefficient Cp is defined as the pressure divided by $0.5\rho U_0{}^2$.

First the mean and fluctuating pressures on a cylinder are shown in Fig. 8. The computed pressure distribution of the oscillating cylinder at Vr = 5.5, 13.5, 24.0 are good agreement with the previous experimental data.

At Vr = 5.5 the negative pressure recovers on the side surface, although the pressure coefficients on a stationary cylinder is constant along the side surface. While, at Vr = 13.5 and Vr = 24.0 the negative pressure on the side surface does not recover, because there is not a reattaching flow as shown in Fig. 6.

Next the contribution of the unsteady pressures to the aerodynamic oscillations is clarified. The unsteady pressure Cp_m is defined as a component of the pressure coefficient at the cylinder oscillation frequency as following equation:

$$Cp_m = Cp0*\sin(2\pi f_m t + \phi) \qquad (23)$$

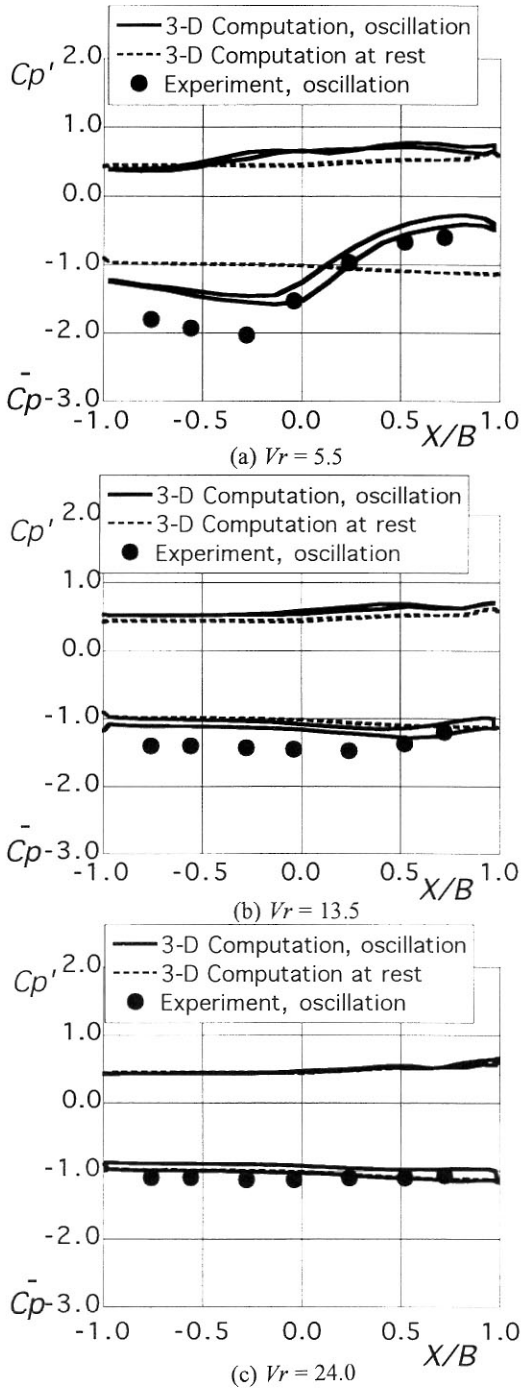

(a) Vr = 5.5

(b) Vr = 13.5

(c) Vr = 24.0

Fig. 8 Distribution of mean and fluctuating pressure on an oscillating cylinder

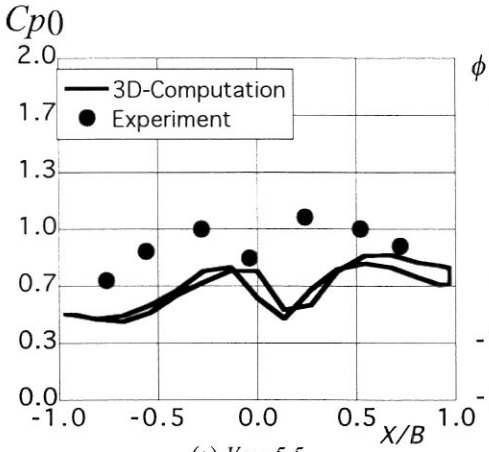

(a) $Vr = 5.5$

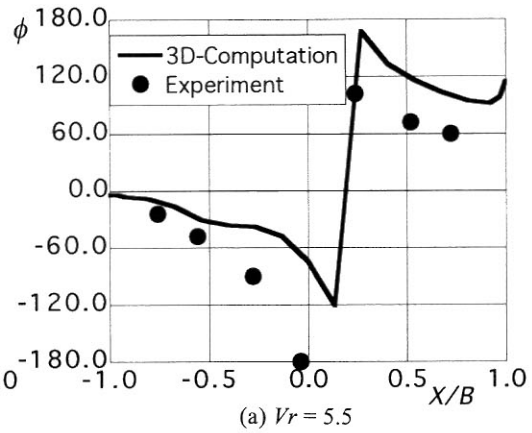

(a) $Vr = 5.5$

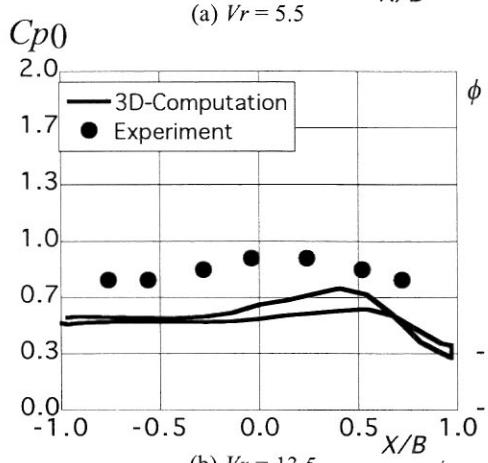

(b) $Vr = 13.5$

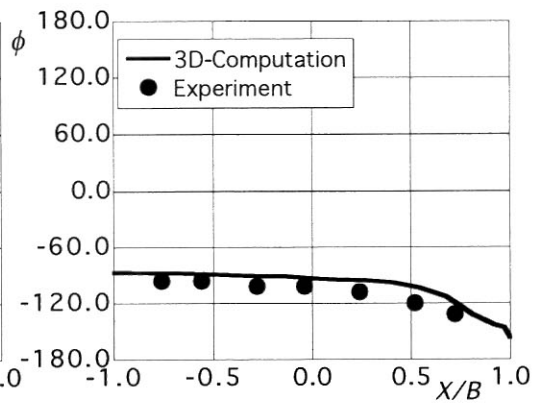

(b) $Vr = 13.5$

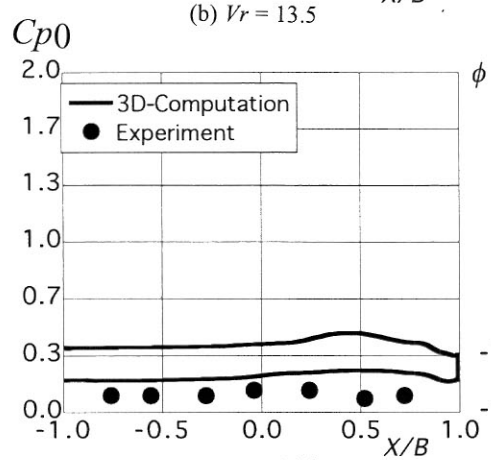

(c) $Vr = 24.0$

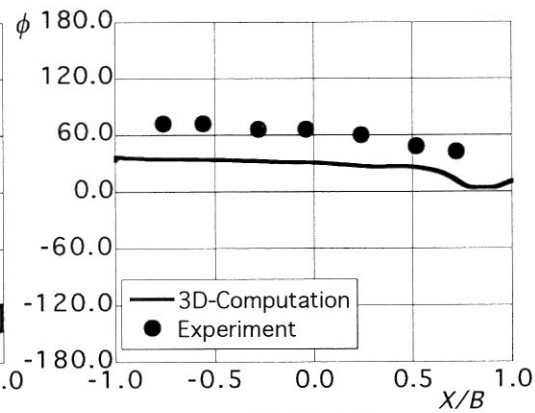

(c) $Vr = 24.0$

Fig. 9 Distribution of amplitude of unsteady pressure on an oscillating cylinder

Fig. 10 Distribution of phase angle between unsteady pressure and cylinder displacement

where $Cp0$ and ϕ stand for the amplitude of the unsteady pressure and the phase angle($-180°<\phi<180°$) by which the suction on the side surface leads the displacement. The total energy distribution of the unsteady pressure during a period is expressed by equation(24).

$$W\,cp = Wcp0 * \sin\phi \tag{24}$$

If $\sin\phi$ is positive, the unsteady pressure is capable of increasing the oscillation. If $\sin\phi$ is negative, it damps the oscillation.

In addition the drag and the lift coefficients are defined as the drag and the lift per unit span divided by $0.5\rho U_0{}^2 B$. Torque coefficient is non-dimensionalized by $0.5\rho U_0{}^2 B^2$. The unsteady lift C_{Lm} is defined as a component of the lift coefficient at the cylinder oscillation frequency as follows:

$$C_{Lm} = C_{Lm0} * \sin(2\pi f_m t + \phi) \tag{25}$$

$Cp0$ and ϕ of the unsteady pressure are presented in Figs. 9 and 10 respectively. Time histories of the drag, the lift and the torque coefficients are shown in Fig. 11.

The distribution of amplitude of the unsteady pressure at Vr = 5.5 has two peaks. Taking the phase angle into consideration, the windward and the leeward peaks have effects of damping and exciting the oscillation respectively. The combination of the two unsteady pressure at Vr = 5.5 generates larger torque coefficient than that of the other reduced velocities. With regard to an unsteady lift there is the force capable of sustaining the vortex-induced oscillation, because the phase angle of lift at Vr = 5.5 is 24.4°.

At Vr = 13.5 and 24.0 the amplitude and the phase angle of unsteady pressure are almost constant along the side surface. Taking the phase angle into consideration, the unsteady pressure at Vr =13.5 damps the oscillation within the range $-180°<\phi<0°$. On the other hand in case of Vr = 24.0 it causes the galloping to appear. These results are confirmed by the fact that the phase angle of lift at Vr = 13.5 and 24.0 are -97.9° and 6.4° respectively.

The distributions of the computed unsteady pressure at Vr = 5.5, 13.5 and 24.0 are good agreement with the experimental ones. According to the time histories in Fig. 11 it is found that the fluctuation of the lift at Vr = 24.0 is not locked on the oscillation of a cylinder. Due to the irregular fluctuation the discrepancy of $Cp0$ between the upper side and the lower side at Vr = 24.0 is larger than that at the other reduced velocities.

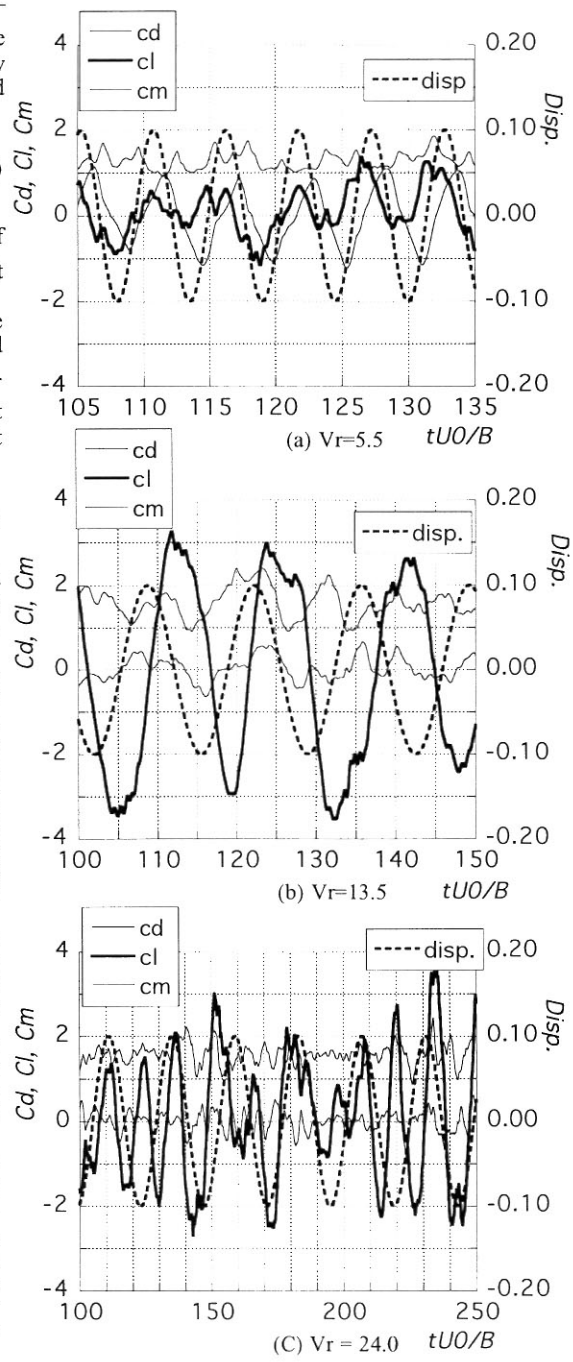

Fig. 11 Time histories of drag, lift and torque coefficients

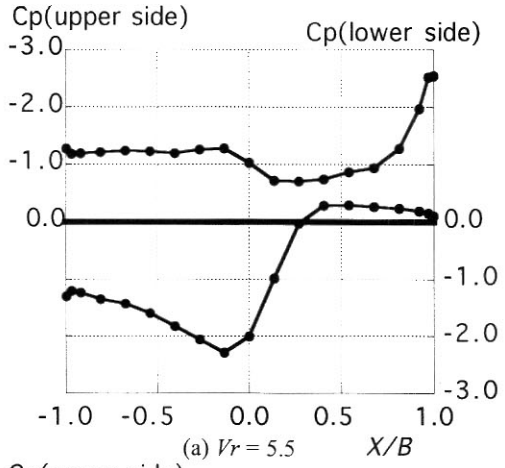

(a) $Vr = 5.5$

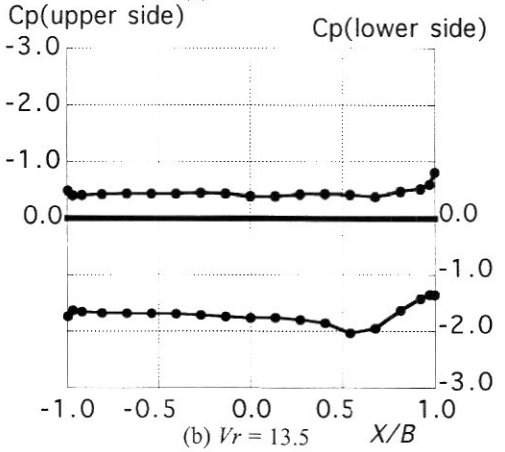

(b) $Vr = 13.5$

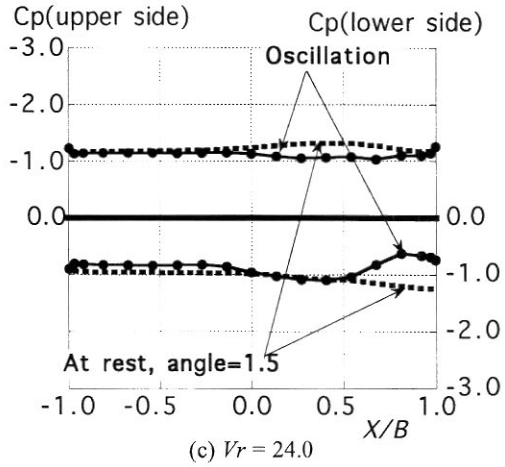

(c) $Vr = 24.0$

Fig. 12 Distribution of phase-averaged pressure on an oscillating cylinder at $2\pi fmt = 0°$

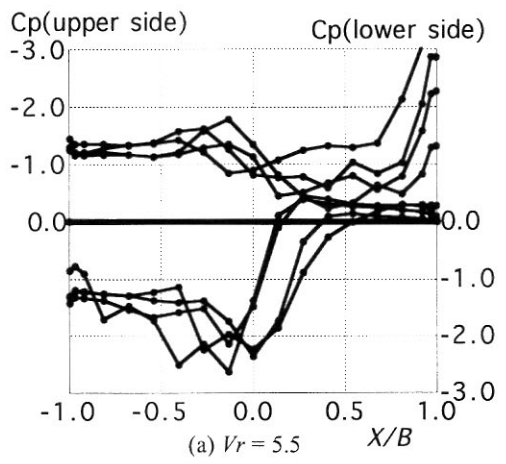

(a) $Vr = 5.5$

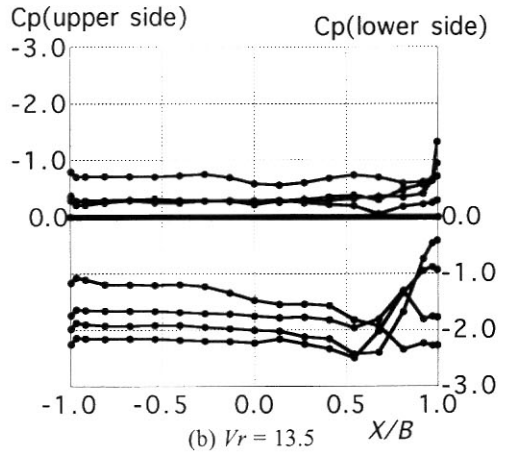

(b) $Vr = 13.5$

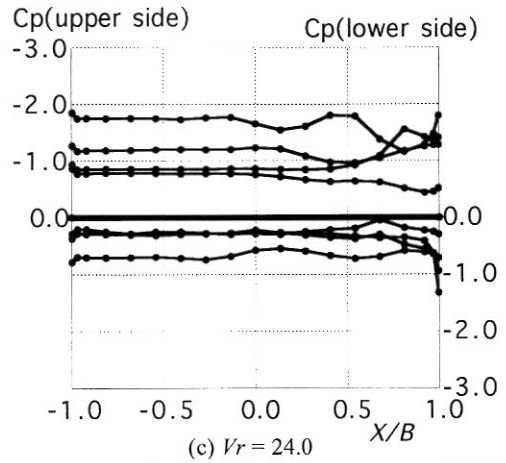

(c) $Vr = 24.0$

Fig. 13 Distribution of instantaneous pressure on an oscillating cylinder at $2\pi fmt = 0°$

6. COMPUTED UNSTEADY AERODYNAMIC FORCES AND WAKE STRUCTURES

The phase-averaged pressure distribution on the side surface of the oscillating cylinder at $2\pi fmt = 0°$(At that time the cylinder is moving upward.) is shown in Fig. 12. Here we focus on the relations between the unsteady pressure distributions on the side surface and the wake structures.

In case of $Vr = 5.5$ the extreme negative low value is found near the trailing edge of the upper side. While on the lower side the negative pressures sharply recover there. Above two characteristics of pressures cause to sustain the vortex induced oscillation. These originate from the collision of vortex core and the reattachment of the separated flow in Fig. 5.

At Vr =13.5 and 24.0 the pressure coefficients are almost constant along the side surface. The magnitude of the negative pressure on the lower side is larger than that on the upper side at $Vr = 13.5$. Therefore the aerodynamic forces have an effect of damping the oscillation. On the other hand at Vr = 24.0 the magnitude of the negative pressure on the upper side is a little larger than that on the lower side. As a result the aerodynamic forces have an effect of unstable oscillations. It is recognized from the wake patterns in Fig. 5 that as the shear layer is closer to the side surface of the cylinder, the magnitude of negative pressure is larger.

In view point of the quasi-steady theory the phase-averaged pressure distribution at $Vr = 24.0$ is compared with the mean pressure distribution of the stationary cylinder with the angle of attack(1.5°). Except near the trailing edge of the lower side the pressure distribution of both cases are as a whole coincident with each other. This computational result confirms that the quasi-steady theory can be applicable to the aerodynamic forces at $Vr = 24.0$.

Fig. 13 shows instantaneous pressure distributions which is four times sampled at $2\pi fmt = 0°$. At Vr = 5.5 and 13.5 because the fluctuation of lift is locked on the oscillation of a cylinder as shown in Fig. 11, the instantaneous pressure distributions do not scatter very much. The tendency of the instantaneous pressures is coincident with that of the phase-averaged pressures. On the other hand at $Vr = 24.0$ although the fluctuation of lift is not lock on the oscillation, it is found that the self-excited force can be simulated as shown in Fig. 13.

7. CONCLUSIONS

Three-dimensional simulations of the flow around the oscillating rectangular cylinder in heaving mode are carried out. The following conclusions are obtained.

1. With regard to the pressure distribution of the side surface of the rectangular cylinder with a section of the depth / width of 2.0 the computational results are good agreement with the experimental ones.

2. At $Vr = 5.5$ the separation bubble on the lower side surface at $2\pi fmt = 0$ and the separated vortices from leading edge on the lower side surface at $2\pi fmt = 90°$ can be observed. The separation bubble has more three-dimensional structures than that of other reduced velocities and rest. The wake structures are two-dimensionalized in other region.

3. At $Vr = 5.5$ the collision of vortex core near the trailing edge of the upper side and the reattaching flow on the lower side at $2\pi f_m t = 0$ are capable of sustaining the vortex-induced oscillation.

4. At Vr = 13.5 and 24.0 the separated flow does not reattach afterbody and forms the wide wake. The three-dimensionality of flow structures inside the separated flow gradually increases toward the leeward of the cylinder.

5. At Vr = 13.5 the aerodynamic forces have an effect of damping the oscillation.

6. Although the flow at Vr = 24.0 is not locked on the oscillation of a cylinder, the each instantaneous pressure distribution on the side surface generates the self-excited force. It is confirms that the quasi-steady theory can be applicable to the aerodynamic forces at $Vr = 24.0$.

REFERENCES

[1] T. Tamura, Y. Itoh, A. Wada and K. Kuwahara, Numerical Investigation on the Aerodynamic Instability of Bluff Cylinders, J. Wind Engrg. Indust. Aerodyn., No. 46&47, 1993.

[2] T. Tamura, K. Tsuboi and K. Kuwahara, Numerical simulation of unsteady flow patterns around a vibrating circular cylinder, AIAA Paper, 88-0128, 1988

[3] T. Tamura, E. Krause, S. Shirayama, K. Ishii and K. Kuwahara, Three-dimensional computation of unsteady flows around a square cylinder, Proc. 11th ICNMFD, Williamsburg, 1988

[4] F. H. Harlow and J. E. Welch : Numerical Calculation of Time-Dependent Viscous Incompressible Flow of Fluid with Free Surface, Phys. Fluid., Vol.8, 1965, pp2182-2189

[5] T. Kawamura and K. Kuwahara : Computation of high Reynolds number flow around a circular cylinder with surface roughness, AIAA paper, 1984, 84-0340

[6] T. Miyata, M. Miyazaki and H. Yamada, PRESSURE DISTRIBUTION MEASUREMENTS FOR WIND INDUCED VIBRATIONS OF BOX GIRDER BRIDGES, ICWE, 1983.

[7] T. Tamura, Y. Itoh and K.Kuwahara, Comutational separated-reattaching flows around a rectangular cylinder, J. Wind Engrg. Indust. Aerodyn., No. 50, 1993.